

**5d photoionization and Auger decay in atomic Pb**S. Urpelainen,<sup>\*</sup> S. Heinäsmäki, M.-H. Mikkilä, M. Huttula, S. Osmekhin, H. Aksela, and S. Aksela  
*Department of Physical Sciences, University of Oulu, P.O. Box 3000, 90014 Oulu, Finland*

(Received 18 May 2009; published 10 July 2009)

We have studied the Pb 5d photoionization and Auger decay spectrum with high resolution using the new FINEST synchrotron-radiation branchline (on the I3 beamline at MAX-laboratory). We analyzed the experimental spectrum with the help of multiconfigurational Dirac-Fock calculations and analyzed the strong correlation properties of the relativistic  $5d_{3/2}$  and  $5d_{5/2}$  subshells. We show that the many-electron phenomena in photoionization and Auger decay can be described through mixing with the  $np(n=7,8,\dots)$  orbitals.

DOI: [10.1103/PhysRevA.80.012502](https://doi.org/10.1103/PhysRevA.80.012502)

PACS number(s): 31.15.A-, 32.80.Fb, 32.80.Hd

**I. INTRODUCTION**

When heavy atoms are ionized with tunable synchrotron radiation and the emitted electrons are measured with high resolution, one obtains detailed information about the effects of relativity and correlation in atomic electrons. The binding energies, correlation properties and decay widths in atomic lead serve as an important reference material for studies of lead clusters and metallic lead.

The low energy part below the 5d ionization thresholds was studied in atomic lead by Süzer *et al.* [1] who analyzed the 6p photoelectron spectrum. Their study confirmed the relativistic nature of Pb ground- and valence-excited states, originating from the large spin-orbit interactions. Synchrotron studies of the valence region have been performed by Krause *et al.* [2]. The metallic Pb, especially the  $5d_{3/2}$  vs  $5d_{5/2}$  branching ratio, has been analyzed more thoroughly, see e.g., Bancroft *et al.* [3] and Barth *et al.* [4].

The region involving the subvalence region has however not received much attention, but the 5d spectra was measured using synchrotron radiation with (in today's standards) moderate resolution by Sandner *et al.* [5] where the origin of the spectral features was also discussed on the basis of multiconfigurational Dirac-Fock calculations.

The electronic structure in atomic lead is characterized by strong relativistic effects, which are visible in the experimental spectra as well as in the simulations as a rather independent behavior of the relativistic subshells pertaining to  $j = l \pm 1/2$ . Also deviations from the independent-particle central-field model are pertinent, as shown by the appearance of satellite structures in the photoelectron and Auger spectra. The origin of these structures can be mostly accounted for by including configuration interaction of the 5d hole states with valence doubly-excited states. In the previous study [5] the correlation satellite structures were proposed to originate due to mixing with the 6d orbitals. Instead we found here that the main contribution to correlation comes via valence doubly excited states from the 6s and 6p orbitals. In addition to the new theoretical predictions we also present new experimental high resolution 5d photoelectron and subsequent Auger-electron spectra and compare these to the calculated spectra.

**II. EXPERIMENT**

The experiments were carried out on the newly built Finnish-Estonian beamline branch FINEST on the undulator beamline I3 at the new 700 MeV MAX-III electron storage ring [6] in MAX-laboratory (Lund, Sweden). In short the beamline uses radiation from an Apple-II type elliptically polarizing undulator and the light is monochromatized using a 6.65 m off-plane Eagle type monochromator manufactured by Bestec GmbH. The monochromator has three different gratings inserted to cover the photon energy region from 4.6 to 50 eV. The FINEST branch line uses a single Au coated toroidal mirror for refocusing the photon beam to the target position. The FINEST branch is designed for experiments in the gas and vapor phase and thus a highly efficient differential pumping is used before the refocusing mirror. The beamline will be described in some more detail elsewhere [7–9].

To produce the atomic Pb vapor a resistively heated oven [10] with a stainless-steel crucible was used. The temperature of the oven was approximately 800 K corresponding to a vapor pressure in the region of  $10^{-4}$  mbar inside the heated volume [11]. The background pressure inside the spectrometer chamber was of the order of  $5 \times 10^{-7}$  mbar during the experiments.

As the measured kinetic-energy region extends to rather low kinetic energies, an electron repeller was used just outside the oven, but inside the thermal shielding so that the repeller potential does not penetrate to the target volume. This was done in order to reduce the amount of thermally excited electrons (and ions) in the interaction region. The repeller was used at a potential of  $-2$  V with respect to the ground potential.

The photoelectron and Auger spectra were recorded at the photon energy of 42 eV using a Pt coated grating with 4200 l/mm ruling and with monochromator entrance and exit slit openings of 950  $\mu\text{m}$ . This corresponds to a photon bandwidth of approximately 10 meV. The electrons were collected using a modified Scienta SES-100 hemispherical electron energy analyzer mounted on a setup built in Oulu [10,12]. The pass energy of the analyzer was chosen to be 10 eV and the entrance slit 0.4 mm (curved) corresponding to an instrumental broadening of approximately 20 meV. The electrons were detected at the magic emission angle of  $54.7^\circ$  with respect to the electric field vector of the synchrotron radiation, which was 99% vertically linearly polarized (perpendicular to the plane of the synchrotron).

<sup>\*</sup>samuli.urpelainen@oulu.fi

For calibrating the binding energy the noble gas Xe was introduced in the chamber via free expansion from the base of the oven until a partial Xe pressure of approximately  $1 \times 10^{-5}$  mbar was reached. The photon energy was calibrated by measuring the autoionizing Ar  $13s'$  line around 15.8 eV. The photon energy was found to differ approximately by 0.5% from the previously reported value obtained from absorption experiments [13]. The transmission function of the analyzer was not calibrated as the emphasis of the study is not in the relative intensities of the lines.

### III. RESULTS AND DISCUSSION

The calculations on the electronic structure and transitions were done within the multiconfigurational Dirac-Fock formalism. The atomic states are taken as eigenstates of parity and total angular momentum  $J$ , expressed as linear combinations of configuration state functions (CSFs). These are constructed as antisymmetrized  $jj$  coupled products of single-particle Dirac orbitals. The bound-state orbital wave functions were obtained using the GRASP92 [14] code (slightly modified to get better convergence properties), whereas the energies and mixing coefficients were computed with the GRASP2K [15] package. After generating the bound electronic states, the photoionization probabilities were estimated within the frozen-core picture, by multiplying the mixing coefficients of the CSFs of final ionic state with the corresponding mixing coefficients of the “parent” CSFs in the ground state. The method has been described, e.g., in [16].

The observed Auger-electron intensity is proportional to  $n_{fn} = 2\pi \sum_{ij} |A_{fn}|^2 |T_{ni}|^2 / P_n$ , where  $A_{fn}$  is the Auger decay amplitude,  $T_{ni}$  the photoionization amplitude, and  $P_n$  the total decay rate of the one-hole state  $n$ . The sum goes over the quantum numbers of the continuum electrons. Here we have used the fact there is only one initial state for the photoionization. The Auger amplitudes were obtained using unpublished routines from the Ratip [17] package.

For the ground state of atomic lead, we found that a good description was obtained by including only the single nonrelativistic electronic configuration  $[\text{Xe}]4f^{14}5d^{10}6s^26p^2$ . The outermost open  $6p$  shell gives rise to five energy levels, having the total  $J$  values 0, 1, 2, 2, 0, in energy order. The calculated splittings with respect to the ground state were (in eVs) 0.839, 1.307, 2.707, and 4.054. These can be compared to the experimental values [18] 0.969, 1.321, 2.660, and 3.653. This means that at the temperature  $\sim 500$  °C used in our experiments, only the lowest neutral level having  $J=0$  was occupied. As a heavy atom, the electronic states in lead are best described within the  $jj$  coupling. This was also reflected by the eigenvectors of the neutral state being composed of almost ( $>90\%$ ) pure  $jj$  coupled CSFs. According to our calculations, in the relativistic notation this lowest level consists of the  $6p_{1/2}^2$  and  $6p_{3/2}^2$  valence electronic configurations, with the weights 0.924 and 0.076, respectively. This also shows that strong spin-orbit interaction makes Pb effectively a closed-shell atom, as reflected by the relatively large energy gap between the ground- and first-excited neutral state. This was already the conclusion of Süzer *et al.* [1]. As

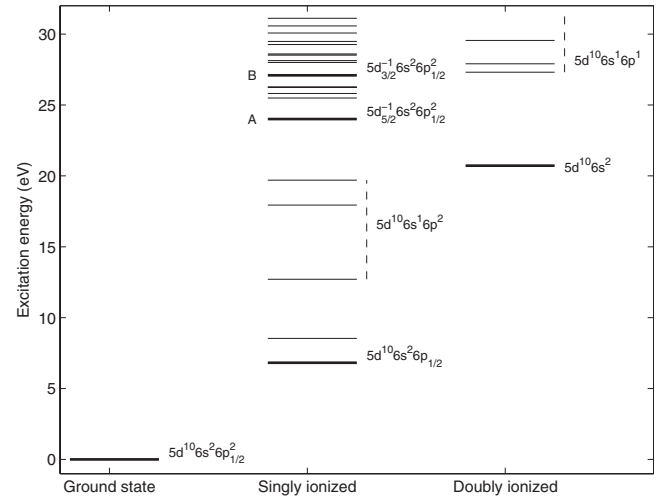


FIG. 1. Calculated energy levels within the single (nonrelativistic) configuration scheme. The leading relativistic configuration of selected levels (printed in bold) is presented. Dashed lines show the energy region spanned by levels originating from the nonrelativistic electronic configurations shown on their right. The doubly ionized levels above the highest singly-ionized level are not shown.

a comparison, the corresponding gap in Sn, with similar valence electronic configuration, is only 0.21 eV [19]. In contrast to [5], in our calculations the inclusion of the  $6d$  orbitals in the ground state did not result in any improvements, and we conclude that its role is negligible.

Let us first discuss the gross features of the  $5d$  ionization and subsequent Auger decay in terms of energy levels constructed from single nonrelativistic electronic configurations. For the singly-ionized state, the nonrelativistic configuration  $5d^96s^26p^2$  gives rise to 16 relativistic configurations with  $J=3/2$  and  $J=5/2$ . For the doubly ionized states, the nonrelativistic configurations  $5d^{10}(6s6p)^2$  give rise to 10 relativistic configurations. The calculated energy levels are depicted in Fig. 1, which for reference also shows the locations of the valence  $6s$  and  $6p$  ionized states. Comparison of the experimental spectrum and the energy-level diagram shows that the single-configuration calculation is able to predict the positions of the energy levels relatively well.

The energy levels show that the part of the  $5d^{-1}$  states between the main components, characterized by  $5d_{5/2}^{-1}6s^26p_{1/2}^2$  and  $5d_{3/2}^{-1}6s^26p_{1/2}^2$  relativistic configurations, is only capable of decaying into the single  $5d^{10}6s^2(^1S_0)$  state, whereas the valence  $6s$  and  $6p$  ionized states decay only by photon emission. The higher-lying  $5d$  hole states have other decay channels, but they have negligible intensity in the photoionization. The calculated photoionization spectrum using the abovementioned configurations is presented in the lowest column of Fig. 2. The major features shown, labeled as “A” and “B,” are the peaks corresponding to the main components  $J=5/2$  at 24.01 eV and  $J=3/2$  at 27.09 eV, respectively. In between the main peaks there are configuration-interaction satellites arising from mixing with the states having electronic configurations  $5d_{3/2}^{-1}6s^26p_{1/2}^16p_{3/2}^1$ . The calculated intensities (peak areas) for the main components have the ratio 1.00:0.59. The deviation from the “geometrical” ratio 3:2 results from larger configuration interac-

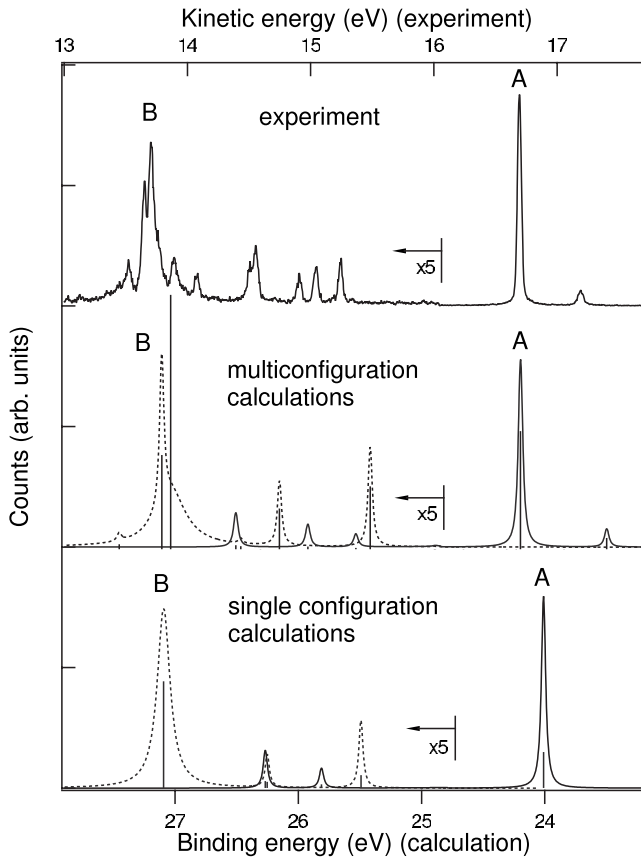


FIG. 2. Experimental and calculated 5d photoionization spectrum within the multi- and single (nonrelativistic) configuration scheme. The transitions corresponding to the  $J=5/2$  ionic states are shown with solid line, while the dashed line shows transitions corresponding to the  $J=3/2$  ionic states. The calculated photoionization probabilities are denoted by sticks, whereas the calculated curves have been generated by taking into account the widths from Auger calculations. The higher binding energy part has been multiplied by 5 for better visualization.

tion of the  $J=3/2$  peak, reducing the intensity in photoionization. The lifetimes of the peaks differ so that the calculated Auger decay width for the  $J=5/2$  component is 1.5 meV but for the  $J=3/2$  component it is 127 meV.

The Auger process within the single nonrelativistic configuration scheme is extremely simple due to the single doubly ionized level  $5d^{10}6s^2(^1S_0)$  reachable by the main components of the singly-ionized states. The Auger spectrum becomes a mirror image of the corresponding photospectrum (Fig. 3). Moreover, the Auger decay amplitudes of the main relativistic configurations contain only one channel and are depicted by  $\langle 5d_J^{-1}6s^26p_{1/2}^2 || V_{ee} || 5d^{10}6s^2(^1S_0) \epsilon d_J \rangle$ , which reduce (in atomic units) to  $\frac{1}{7}R^3(6p_{1/2}, 6p_{1/2}; 5d_{5/2}, \epsilon d_{5/2})$  for  $J=5/2$  and to  $\frac{1}{3}R^1(6p_{1/2}, 6p_{1/2}; 5d_{3/2}, \epsilon d_{3/2})$  for  $J=3/2$ . Here  $R^k$  denotes the relativistic Slater integral. Thus, ignoring mixing and small changes in orbital functions, the differing lifetimes have a natural geometrical interpretation: angular-momentum conservation only allows for the smaller  $R^3$  integral in the decay of the  $J=5/2$  component versus the larger  $R^1$  integral in case of the  $J=3/2$  level.

Comparing the calculated single configuration spectrum and the experimental spectrum in Fig. 2 shows that there are

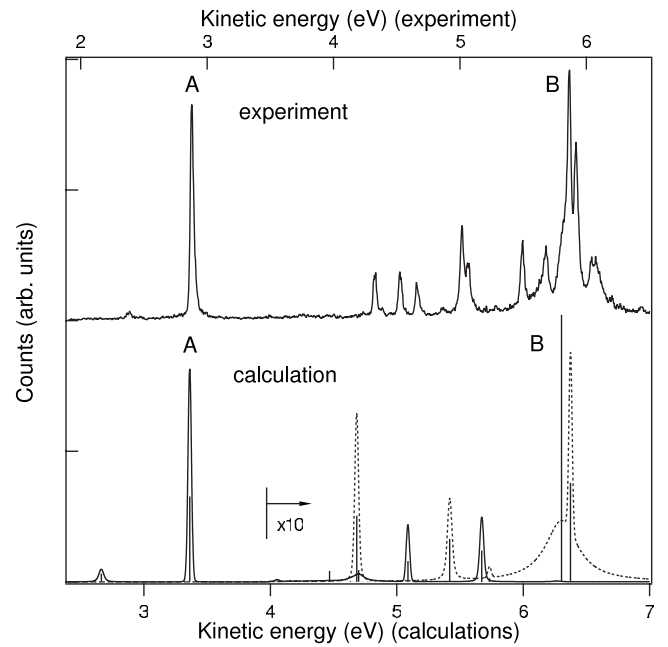


FIG. 3. Experimental and calculated 5d Auger spectrum. Mixing with  $7p$  and  $8p$  included. Equal width 40 meV for all peaks except for the main  $J=3/2$  peak at 27.04 eV binding energy where the calculated width 300 meV has been used. The solid and dashed lines correspond to the  $J=5/2$  and  $J=3/2$  final ionic states, respectively. In addition, the calculated rates are depicted by sticks. The high kinetic-energy part of the calculated spectrum has been multiplied tenfold for visualization.

additional structures which go beyond the single configuration scheme. Especially the main  $J=5/2$  peaks is associated with a satellite with lower binding energy and the main  $J=3/2$  peak is associated with several other energetically close transitions. In the work of Sandner *et al.* [5] the origin of these transitions was discussed on the basis of including the  $6d$  orbitals, but according to our analysis they do not seem to play any appreciable role. A natural extension instead is to consider the effect of configuration interaction with valence doubly-excited states, which cannot by themselves be directly ionized when configuration interactions are not taken into account. The energy-level diagram in Fig. 1 shows that the main singly-ionized  $J=3/2$  component (B) is energetically close to doubly ionized states with electronic configurations  $5d^{10}6s^16p^1$ . It is therefore natural to suggest that mixing with  $5d^{10}(6s6pnl)^3$  type of configurations should be taken into account. In our calculations it turned out that including configuration interaction with levels coming from  $nl=7p, 8p$  accounted for most of the features seen in the experiment. The mixing changes the situation so that the singly-ionized spectrum becomes energetically wider and produces new satellite structures in the spectrum due to mixing of configurations.

The main calculated parameters are affected so that in the multiconfigurational calculation the intensity ratio of the main peaks becomes 1.00:0.43 and the half-width of the  $J=3/2$  component becomes 303 meV, more than twice the single configuration calculation result. These effects can be understood on the basis of increased mixing which reduces

the photoionization intensity but at the same time allows for more decay channels having relatively large amplitudes of the form  $\langle 6pnp || V_{ee} || \epsilon d6s \rangle$ . However the calculated widths of the peaks suffer from uncertainties pertaining to the numerical generation of continuum orbitals with very low energy.

The calculated photoionization spectrum within the multiconfigurational calculation is shown in the middle column of Fig. 2. The most prominent new features are the appearance of the new peak at binding energy 23.50 eV. This transition is interpreted as a configuration-interaction satellite arising from mixing of the main  $J=5/2$  configuration  $5d_{5/2}^{-1}6s^26p_{1/2}^2$  with the  $5d^{10}6s^16p_{1/2}^17p_{3/2}^1$  configuration. Multiconfiguration calculation also predicts additional peaks between the main peaks A and B, even though it does not fully reproduce the manifold peak structure around the main  $J=3/2$  peak B.

The qualitative features of the Auger emission do not change in the multiconfigurational calculation. This stems from the fact that for most of the states in the photoelectron spectrum the decay to the  $5d^{10}6s^2(^1S_0)$  remains the only decay channel and therefore the theoretical Auger spectrum is again the mirror image of the photoelectron spectrum. Small changes from the “mirroring” are induced by the energy dependence of the continuum waves which affect the Auger amplitudes. Higher intensity of the  $J=5/2$  main peak A in Auger as compared to photoelectron spectrum cannot be confirmed by our experiment, as the transmission of the spectrometer drops dramatically at very low kinetic energies and the intensity ratio to the next peak is highly uncertain. Detecting the spectrum with an electron time-of-flight spectrometer might help in clarifying if theory is correct here.

In our calculations we noticed that in the low binding energy part of the photoelectron spectrum, dominated by the  $5d_{5/2}$  type hole states, the inclusion of the  $7p$  orbital can account for most of the features, whereas toward the higher binding energies corresponding to hole states with predominantly  $5d_{3/2}$  character, the inclusion of the  $8p$  orbital makes the correspondence with the experimental spectrum better. The experimental spectrum shows in this region a number of transitions which we were not able to fully simulate due to numerical uncertainties, but which most likely (based on the energy-level structures shown in Fig. 1) are due to configuration mixing of the  $5d_{3/2}^{-1}6s^26p_{1/2}^2$  and various states resulting from  $5d^{10}6s^16p_{1/2}^1n_l^1$  type of configurations. The differing behavior of the peaks A and B also reflects the fact that strong spin-orbit interaction in lead makes the relativistic subshells quite independent of each other.

In addition to the direct ionization from the  $5d_{3/2,5/2}$  shells and mediated through configuration interaction, included in our Auger amplitudes used in the computations, various many-electron transitions can populate the doubly-excited valence ionic states. In these shake up and conjugated shake off transitions the dipole single-electron transitions are accompanied by monopole transitions (overlaps) of other orbitals. Based on our analysis, the many-electron transitions are responsible for at most 10% of the intensity of the satellite peaks, and the most part thus comes through configuration interaction.

#### IV. CONCLUSIONS

The ionization and subsequent Auger decay of the Pb  $5d$  shell are characterized by strong relativistic effects originating from the large spin-orbit splitting of the relativistic  $5d_{3/2}$  and  $5d_{5/2}$  subshells. The splitting separates the energy levels and pushes the higher-lying  $5d_{3/2}$  shell into a region where the single-hole state becomes energetically close to valence doubly-ionized levels. This causes the deviations from the independent-particle model which, in the MCDF calculations, manifest themselves as strong configuration-interaction effects. They cause the  $5d$  hole states to be mixed with  $p$ -type Rydberg orbitals, and the photoelectron and Auger spectra show numerous extra structures originating from this mixing.

The results concerning the behavior of the  $5d$  subshells can serve as a starting point in analyses of spectral features in larger systems containing lead. Especially in clusters the important question is the formation of first molecular orbitals and eventually (valence) band structures. It is likely that the more weakly bound  $5d_{5/2}$  subshell participates in the formation of molecular orbitals earlier than the  $5d_{3/2}$  component. Also the differing electron-electron interactions of these atomic orbitals are likely to play a role so that the composition of the extended (molecular) orbitals in larger systems shows the differences visible in atomic lead.

#### ACKNOWLEDGMENTS

This work has been financially supported by the Research Council for Natural Sciences of the Academy of Finland. S.U. would like to thank the Vilho, Yrjö, and Kalle Väisälä Foundation, the Tauno Tönnning Foundation, and Magnus Ehrnrooth Foundation for financial support. We acknowledge the staff of MAX-laboratory for their assistance during the experiments.

- 
- [1] S. Süzer, M. S. Banna, and D. A. Shirley, *J. Chem. Phys.* **63**, 3473 (1975).  
 [2] M. O. Krause, P. Gerard, and A. Fahlman, *Phys. Rev. A* **34**, 4511 (1986).  
 [3] G. M. Bancroft, W. Gudat, and D. E. Eastman, *Phys. Rev. B* **17**, 4499 (1978).  
 [4] J. Barth, F. Gerken, C. Kunz, V. Radojevic, M. Idrees, and W. R. Johnson, *Phys. Rev. Lett.* **55**, 2133 (1985).  
 [5] N. Sandner, V. Schmidt, W. Mehlhorn, F. Wuilleumier, M. Y. Adam, and J. P. Desclaux, *J. Phys. B* **13**, 2937 (1980).  
 [6] M. Sjöström, E. Wallén, M. Eriksson, and L.-J. Lindgren, *Nucl. Instrum. Methods Phys. Res. A* **601**, 229 (2009).  
 [7] S. Urpelainen, Ph.D. thesis, University of Oulu, Oulu Finland (unpublished).  
 [8] M. Patanen, S. Urpelainen, M. Huttula, R. Sankari, E. Nömmä, and M. Manninen, *Phys. Rev. A* **80**, 012502 (2009).

- miste, E. Kukkk, H. Aksela, and S. Aksela, Phys. Rev. A (to be published).
- [9] T. Balasubramanian *et al.* (unpublished).
- [10] M. Huttula, S. Heinäsmäki, H. Aksela, E. Kukkk, and S. Aksela, J. Electron Spectrosc. Relat. Phenom. **156–158**, 270 (2007).
- [11] R. E. Honig and D. A. Kramer, RCA Rev. **30**, 285 (1969).
- [12] M. Huttula, M. Harkoma, E. Nömmiste, and S. Aksela, Nucl. Instrum. Methods Phys. Res. A **467–468**, 1514 (2001).
- [13] K. Yoshino, J. Opt. Soc. Am. **60**, 1220 (1970).
- [14] F. A. Parpia, C. F. Fischer, and I. P. Grant, Comput. Phys. Commun. **94**, 249 (1996).
- [15] P. Jönsson, X. He, C. F. Fischer, and I. P. Grant, Comput. Phys. Commun. **177**, 597 (2007).
- [16] M. Huttula, E. Kukkk, S. Heinäsmäki, M. Jurvansuu, S. Fritzsche, H. Aksela, and S. Aksela, Phys. Rev. A **69**, 012702 (2004).
- [17] S. Fritzsche, J. Electron Spectrosc. Relat. Phenom. **114–116**, 1155 (2001).
- [18] D. Wood and K. L. Andrew, J. Opt. Soc. Am. **58**, 818 (1968).
- [19] W. G. Brill, Ph.D. thesis, Purdue University, 1964.